

A Wideband Frequency Beam-Scanning Antenna Array for Millimeter-Wave Industrial Applications

Abdul Jabbar, *Graduate Student Member, IEEE*, Jalil Ur-Rehman Kazim, *Graduate Student Member, IEEE*, Zhibo Pang, *Senior Member, IEEE*, Muhammad Ali Babar Abbasi, *Senior Member, IEEE*, Qammer Abbasi, *Senior Member, IEEE*, Muhammad Ali Imran, *Fellow, IEEE*, and Masood Ur-Rehman, *Senior Member, IEEE*

Abstract— In this article, a compact, wideband, and high-gain frequency beam-scanning planar antenna array is presented at 60 GHz ISM band with enhanced performance. Unlike conventional series-fed arrays, which frequently exhibit limited bandwidth, the suggested antenna utilizes a modified series-fed microstrip patch array with finite tapering and finely tuned to resonate at multiple frequencies within the desired band to attain broad-spectrum capabilities. First, a wideband 8-element linear antenna array is designed that provides -10 dB impedance bandwidth of 41.52% (54–82.3 GHz) covering the entire 60 GHz millimeter-wave (mmWave) ISM band from 57–71 GHz. The linear array produces fan-beam patterns, and has a peak realized gain of 13.48 dBi at 64 GHz, with less than 1 dB gain variation within the entire 57–71 GHz. Then, the proposed linear array is employed as a sub-array in a hybrid parallel-series topology to design a compact and high-gain 64-element (8×8) planar array. The planar array covers entire 57–71 GHz band with the peak measured gain of 20.12 dBi at 64 GHz and less than 1 dB gain variation within 57–71 GHz, thereby providing 1 dB gain bandwidth of 14 GHz. The planar array provides narrow directional beams with an average half-power beamwidth of 9.7° and 11.78° in the elevation and azimuth planes respectively, for point-to-point multi-gigabit mmWave connectivity. The phase variation of the series-fed topology is employed to produce frequency beam-scanning range 40° in 57–71 GHz band, which is experimentally elucidated. The array prototypes are fabricated and measured. The measured and simulated results show reasonably good agreement, thus validating the performance of the proposed antenna array for 60 GHz mmWave ISM band applications.

Index Terms—60 GHz mmWave antenna array, frequency beam-scanning, Industrial IoT, mmWave communication.

I. INTRODUCTION

THE next-generation industrial wireless communication and sensing networks require ultra-reliability, extremely low latency, high throughput, and finer-grain spatial differentiation. Traditional wired networks suffer through serious impediments such as expensive installation and maintenance costs, restricted mobility, reduced flexibility, and

a lack of reconfigurability in a dynamic industrial environment. Moreover, legacy sub-6 GHz industrial, scientific, and medical (ISM) bands (2.4 and 5 GHz) cannot fully meet the requirements of high speed, high bandwidth (BW), and low latency. In this view, the 60 GHz unlicensed millimeter-wave (mmWave) ISM band is envisaged as a potential enabler to boost the performance of next-generation industrial wireless networks due to its huge available BW of 14 GHz from 57 to 71 GHz [1], [2] and compact radio/antenna size [3]. The 14 GHz band is divided into six channels, each with 2.16 GHz BW. The wide available BW paves the way for a wide variety of emerging industrial applications such as the Industrial Internet of Things (IoT), cyber-physical systems, intelligent factory logistics, flexible manufacturing, autonomous mobile robots (AMRs), autonomous guided vehicles (AGVs), remote visual monitoring and surveillance, image-guided automated assembly, high-definition video surveillance and control, and high-speed wireless backhaul [4]–[10].

Since the mmWave signals propagate in a quasi-optical manner, with the transmitted power reaching the receiver side via line-of-sight (LOS) paths or low-order reflected paths, thus the contribution of diffracted components is insignificant and path loss is quite dominant [9]. Additionally, since the oxygen absorption is maximum around 60 GHz, it necessitates the design of high gain antenna arrays to mitigate the undesired path loss as well as to enhance the communication link budget [11].

At mmWave bands, microstrip printed circuit board (PCB)-based antennas are one of the favoured solutions because of their planar geometry, low cost, ease of fabrication, and ease of integration with radio frequency frontend circuitry. Several PCB-based mmWave antennas aiming for high gain and compact sizes have been presented in the literature [12]–[25] to list but a few. However, achieving wide impedance BW and high gain flatness over a wide frequency band is quite challenging with microstrip PCB antennas. Note that a 3 dB loss (drop) in antenna gain would mean a 50% loss of power. In [12], a substrate integrated waveguide (SIW) leaky wave PCB antenna is reported to cover 55–65 GHz band, however its gain showed more than 2 dB variations in the band. Moreover, planar SIW antennas require metallized vias which increase the fabrication complexity. In [22], a high-efficiency 60 GHz microstrip antenna was presented but with limited BW and more than 3 dB gain variation in the band of interest. Series-fed microstrip patch arrays provide a compact geometry

(Corresponding author: Abdul Jabbar)

Abdul Jabbar, Jalil Ur-Rehman Kazim, Qammer Abbasi, Muhammad Ali Imran, and Masood Ur-Rehman are with James Watt School of Engineering, University of Glasgow, UK (email: abdul.jabbar@glasgow.ac.uk).

Zhibo Pang is with Automation Technology, ABB, Vasteras, Sweden (e-mail: pang.zhibo@se.abb.com).

Muhammad Ali Babar Abbasi is with Center of Wireless Innovation, Queen's University Belfast, UK (e-mail: m.abbasi@qub.ac.uk).

and simpler feed mechanism at mmWave bands. 60 GHz arrays were proposed in [15], [24], [25], but their reported -10 dB reflection BW was lower than 62 GHz with large gain fluctuations in the band. A 60 GHz series-fed antenna array is reported in [25] using Chebyshev tapering distribution, however, its -10 dB impedance BW is limited to 4.2% (58.5 to 62 GHz) with more than 2 dB gain variation in the band. It is inferred from the literature that achieving wide antenna BW while maintaining the high flat gain over 57–67 GHz with planar microstrip patch-based PCB antennas is quite challenging as well as desirable.

A. Design Methodology and Contribution

This article considers aforementioned problems in the context of wideband coverage, high flat gain, and low-cost patch antenna array based on planar PCB technology. Significantly improved operating bandwidth, narrow beamwidth, high efficiency, and low cross-polar levels (x-pol) were achieved with 1 dB gain BW of 14 GHz (57–71 GHz), by implementing the proposed finite tapering of patches in series-fed topology.

Microstrip patch antennas are inherently narrowband [26]. One possibility to increase the impedance BW is to increase substrate thickness while lowering the quality factor to overcome the narrow BW restriction. However, increased surface waves, increased antenna dimensions, and losses would be the cost. Additionally, the stronger surface waves would alter the antenna radiation pattern, and interact with other electronics on the same substrate, and potentially affect the feeding structure of the antenna which is not favorable at the 60 GHz band. Moreover, in order to maintain a simpler design for the 60 GHz band and minimize design intricacies, we refrained from incorporating inset cuts or slots, additional parasitic patches, or any defective ground structures into the design. Therefore, rather than matching a single patch antenna element to a narrow frequency band, we employ the technique of increasing the number of impedance resonances inside the desired band to achieve a wide impedance matching in 57–71 GHz band.

In this work, extensively optimized finite tapered patch elements are loaded to the first element and connected through a thin series-connected microstrip transmission line (MTL). Thus, our proposed methodology involves two prime aspects, first to tune the antenna with multiple resonances within the band of interest, and secondly to optimize tapering of element width in a way to maintain wide impedance matching with low gain fluctuations over a wide BW.

First, a wideband 1×8 linear antenna array is designed by extensive optimization of the tapering ratio of 7 patch elements loaded to the first patch. Contrary to the conventional uniform distribution, binomial distribution [26], or Chebyshev distribution [25] of series-fed arrays, the proposed finite tapering method significantly enhanced the impedance BW covering the entire 57–71 GHz ISM band with high flat gain greater than 12.49 dBi over entire 57–71 GHz. The antenna manifests frequency beam-scanning range of $+40^\circ$ in 57 to 71 GHz band which is experimentally elucidated. The proposed linear array offers a fan-beam radiation pattern is applicable in point-to-multipoint

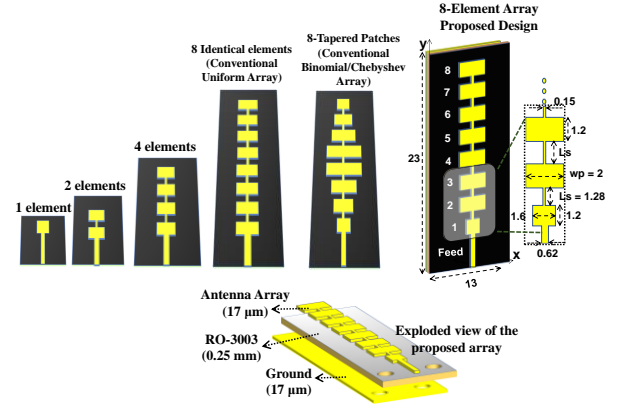


Fig. 1. Design evolution steps and geometry of the proposed 1×8 series-fed array (dimensions in mm).

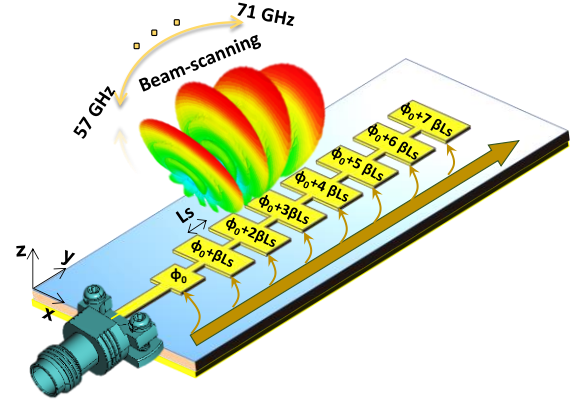


Fig. 2. Illustration of the wave formation across the antenna aperture. The total phase shift along the y-coordinate is contributed by the phase accumulation βLs of the guided wave propagation. The varying net phase relative to the operating frequency results in frequency beam-scanning in the y-z plane

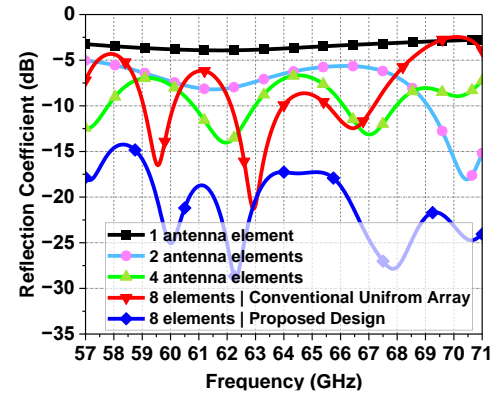


Fig. 3. Reflection coefficient for loading different numbers of series-fed patch antenna elements (1, 2, 4 and 8 elements).

connectivity in various mmWave industrial applications such as wireless personal area networks, Industrial IoT, AGVs, AMRs, object detection, and frequency-modulated continuous wave (FMCW) radars. Then, using an 8-way parallel divider, the proposed 1×8 array was utilized as a sub-array to design a planar 8×8 (64-element) array, that provides high flat gain (realized gain greater is than 19.3 dBi in 57–71 GHz) with directional beams for point-to-point mmWave links. By utilizing this approach, each 1×8 linear array serves as a sub-

array, contributing to the design of compact planar array.

II. DESIGN AND ANALYSIS OF WIDEBAND LINEAR (1×8) ARRAY

The design philosophy and geometry of the proposed antenna are demonstrated in Fig. 1. A preliminary simulated design is reported in [27], however gain variation was more than 2.5 dB above 67 GHz with less than 80% radiation efficiency. In this work, the antenna is designed using high-performance Rogers 3003 laminate substrate with a dielectric constant of 3, having a thickness of 0.25 mm, and copper thickness of 17 μm . Initially, a quarter-wavelength patch with a length of 1.2 mm (less than $\lambda_0/4$ to accommodate fringing effects) and a width of 1.6 mm. A full ground plane was used at the bottom of the substrate to achieve a broadside radiation pattern. The antenna was fed using an edge-launched solderless V-connector, as shown in Fig. 2.

Contrary to the conventional uniform distribution [24], binomial distribution, or Chebyshev distributions [25], the tapering of the other 7 patches (patches 2 to 8) was optimized to 2 mm (instead of 1.6 mm width of patch 1), which we call here as finite tapering. The input impedance of each patch is loaded with the series-fed MTL and the patch next to it, which varies with operating frequency. Initially, the impedance of the single patch element was found to be around 210 Ω . By loading the initial patch element to the seven other optimized patches and seven optimized MTLs, the impedance characteristics of each patch element undergo changes, including varying phases. This dynamic behavior leads to the emergence of different resonant modes in close spectral proximity, such as at 57.1, 60.04, 62.31, 67.81, and 70.61 GHz in case of the proposed array design. Consequently, the antenna array achieves a broad -10 dB impedance matching, while achieving an overall average input impedance of 50 Ω . The series MTL has an optimized width of 0.15 mm (must be within fabrication limits) and length (L_s) of 1.28 mm.

The effect of loading various patches (patch 2 to patch 8) on the reflection BW is shown in Fig. 3. It can be noticed that with all identical patch elements (i.e., the case of the uniformly distributed array), -10 dB impedance BW was limited and resonating at some points with low BW. Similarly, as tapering (of width) was increased towards the center of the array (i.e., $w_p = 2.2, 2.4, 2.6$ mm which tends to be the case of binomial/Chebyshev distribution), the BW becomes quite smaller (less than 2 GHz). However, with the proposed design approach of finite tapering, the entire 57–71 GHz band is covered.

While some intuition may be used in the design process, the properties of the element are not independently modified through a single dimension. Instead, extensive parametric optimizations were run on the array based on full-wave numerical simulations to achieve the desired BW and gain performance. The dimensional optimization showed that the impedance BW is sensitive as a function of the length of the series MTL as well as the width of tapered patches. The effect of the tapering width (w_p) of the patch elements and length (L_s) of the series-connected MTL on impedance BW is shown in Fig. 4(a) and (b) respectively. Note that in Fig. 4(a), one of the curves for $w_p = 2$ mm corresponds to all identical elements

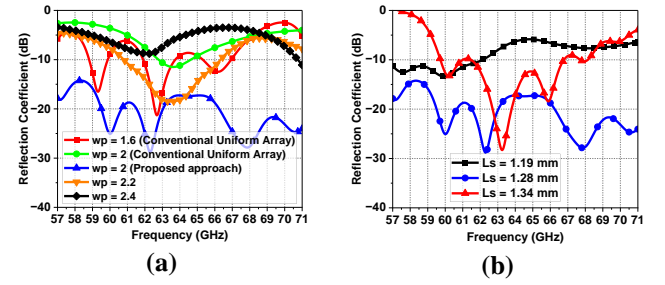


Fig. 4. (a) Effect of width tapering on -10 dB impedance BW of the proposed 1×8 array (b) Effect of change in the length of series-connecting MTL array.

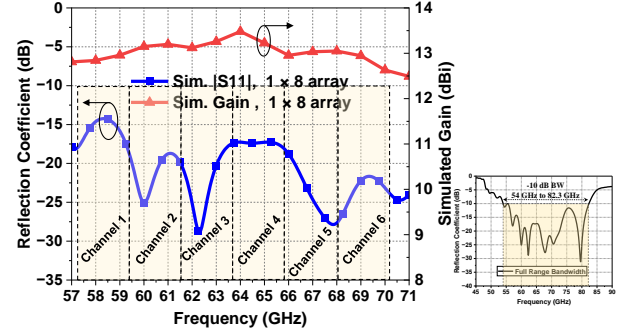


Fig. 5. Simulated reflection coefficient and realized gain of the proposed 1×8 sub-array. Miniaturized figure shows full range reflection coefficient.

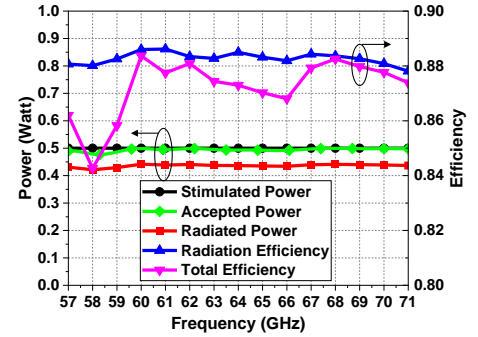


Fig. 6. Simulated power profile, radiation efficiency, and total efficiency of the proposed 1×8 array.

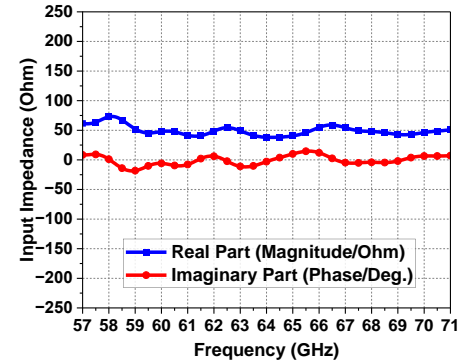


Fig. 7. Input impedance of the proposed 1×8 array. The real part is around 50 Ohm while phase is around across 57–71 GHz band.

including first patch element, which becomes the case of conventional uniform distributed array, and showed limited BW and high gain fluctuation.

The optimized simulated reflection coefficient (-10 dB

impedance BW) and realized gain of the proposed 1×8 array are shown in Fig. 5. The -10 dB impedance BW is 54–82.3 GHz covering all 6 channels of the 60 GHz ISM band and provides a peak gain of 13.48 dBi at 64 GHz. The realized gain is above 12.36 dBi in 57–71 GHz, thereby providing less than 1 dB gain variation in the desired band of interest. As shown in Fig. 6, for an input stimulated signal of 0.5 W, the accepted power is above 0.477 W throughout 57–71 GHz. The radiated power varies between 0.421 W to 0.441 W, which results in above 87.81% radiation efficiency and above 84.26% total efficiency in the whole 57–71 GHz band. Note that radiation efficiency is the ratio of the radiated power to the accepted power, whereas total efficiency is the ratio of the radiated power to the input stimulated power which also accounts for losses due to mismatch. The average input impedance of 1×8 linear array has a real value of around 50 Ω while the average imaginary part is around zero across 57–71 GHz, as shown in Fig. 7, which reveals wideband impedance matching of the proposed array.

The 3-D radiation patterns at various frequency points are shown in Fig. 8(a) and (b). A fan-shaped radiation pattern is observed with a wider half-power beamwidth (HPBW) in the azimuth plane (x-z/ ϕ 0°) ranging between 63.44° to 77° in the band, as shown in Fig. 8(a) and Fig. 9(a). A relatively narrow HPBW is achieved in the elevation plane (y-z/ ϕ 90°) ranging between 12° to 14°, as shown in Fig. 8(b) and Fig. 9(b). This is due to the linear geometry of the array in which the radiation pattern is squeezed along the direction of elements while expanding in the orthogonal direction. The array is broadside at 64 GHz. The side-lobe levels (SLL) are below -10 dB in both planes with very low (x-pol) levels, as revealed in Fig. 9. The electric field heatmap of the proposed linear array at different frequency points is shown in Fig. 10. It can be noted that fringing fields are stronger at the edges of all the patches which result in high flat gain over the wide BW.

A. Frequency Beam-Scanning Analysis

It is instructive to mention here that the main beam direction shifts from -23° (at 57 GHz) towards +17° (at 71 GHz) in the elevation plane. The beam-scanning is due to the phase variation along the series-fed elements at each operating frequency as ϕ , $\phi + \beta L$, $\phi + 3\beta L$, ..., $\phi(n-1)\beta L$, where ϕ is the reference phase at the first element and n is a total number of elements of the array. In fact, βL is the electrical length that adds a phase shift along the direction of the array. Here, $\beta = 2\pi / \lambda_g$ is the phase constant of the propagation wave and is a frequency-dependent parameter. It indicates how the phase of the wave changes as it travels through a medium. L represents the length of the path (MTL) over which the wave propagates. For each operating frequency, the parameter β alters, leading to a change in the total accumulated phase across the antenna aperture at that frequency. Thus, the total phase shift along the y-coordinate (where elements are arranged in series) is contributed from the phase accumulation βL of the wave propagation which results in the frequency beam-scanning phenomenon.

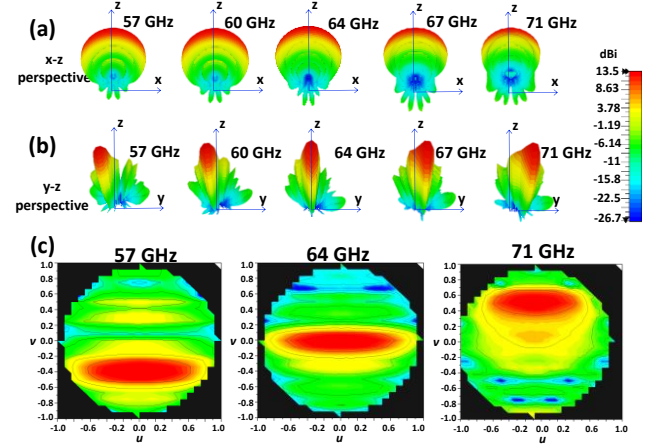


Fig. 8. (a and b) 3-D radiation patterns of the proposed 1×8 array in 57–67 GHz band from two different angular perspectives. Fan-beam can be observed with wider beamwidth in one plane. (c) The u-v orthographic projection reveals fan-beam with frequency beam-scanning performance.

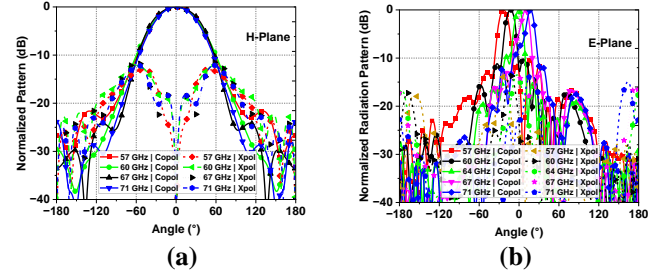


Fig. 9. Rectangular plots of simulated radiation patterns of the proposed 1×8 array across 57–71 GHz band. (a) in H-plane (x-z/ ϕ 0°). (b) in E-plane (y-z/ ϕ 90°).

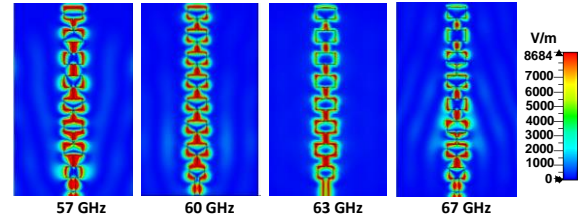


Fig. 10. Electric field distribution of the proposed 1×8 array at different frequency points.

The u-v heat maps in Fig. 8(c) reveal that the main beam shifts in the elevation plane with the change in operating frequency. The u-v projection method projects the 3-D radiation pattern onto the azimuth plane (u-plane) and the elevation plane (v-plane). Essentially, it flattens the radiation pattern, creating two separate 2-D representations to visualize the radiation pattern more intuitively.

III. DESIGN AND ANALYSIS OF 8×8 PLANAR ARRAY

The high gain of the antenna array translates into a reduction of the transmit power needed for a given link performance and enhances signal-to-noise ratio (SNR) at the receiver end. Thus, in a harsh industrial environment, the high gain array at 60 GHz is crucial to mitigate path loss and facilitates reliable communication over a distance of tens of meters. To design a compact and high-gain array, an 8-channel

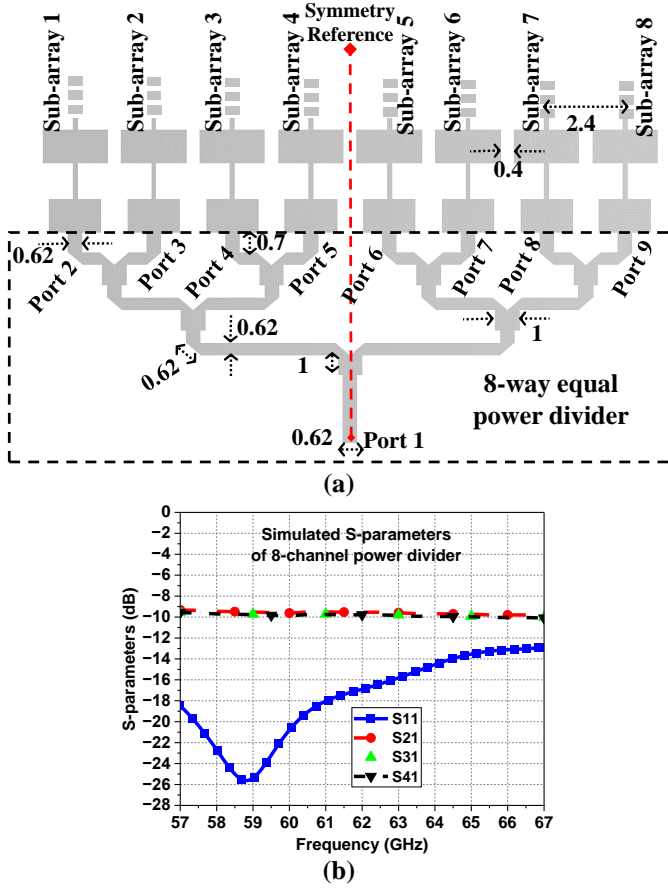


Fig. 11. (a) Schematic of 8-way equal power divider to excite 8 sub-arrays in a parallel-series topology (dimensions in mm). (b) Scattering parameters of the power divider.

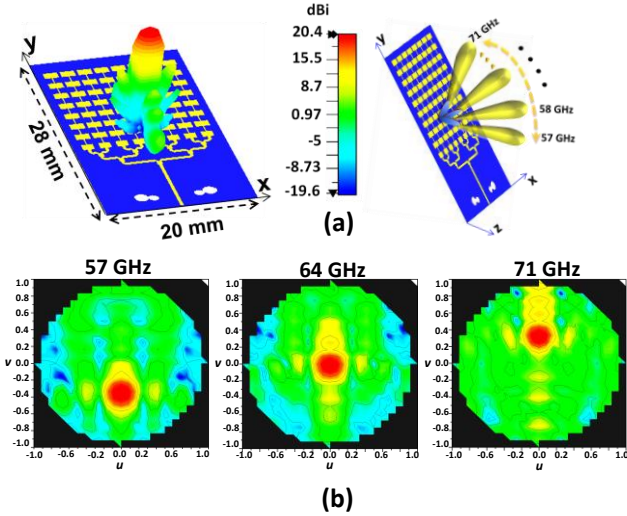


Fig. 12. (a) 3-D simulated schematic design of the proposed 64-element array from CST microwave studio with broadside beam at 64 GHz. (b) uv heat maps at different frequencies demonstrating beam-scanning in the elevation plane.

equal power divider is designed and integrated with the proposed 1×8 sub-arrays at each output port of the divider, as shown in Fig. 11(a). In this way, each proposed 1×8 linear array acts as a sub-array to design a compact 64-element (8×8) planar array.

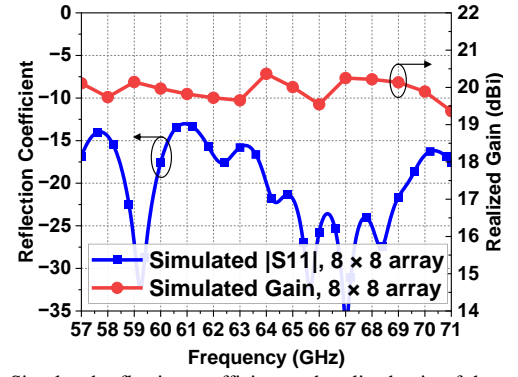


Fig. 13. Simulated reflection coefficient and realized gain of the proposed 8×8 array.

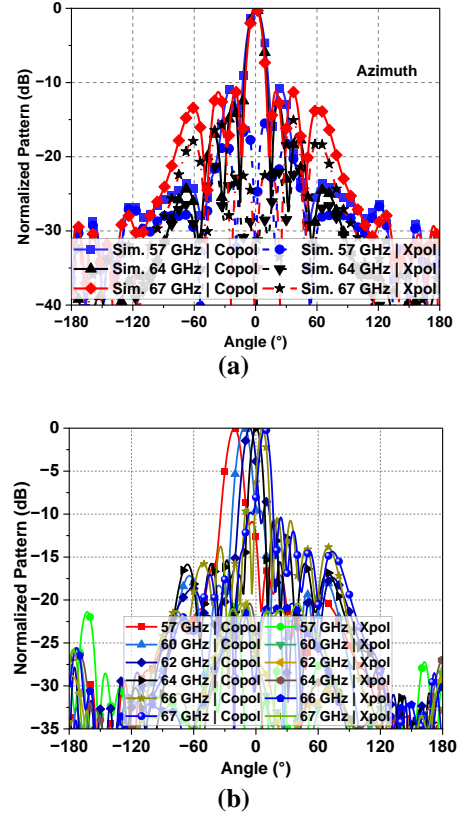


Fig. 14. Simulated normalized radiation patterns of 8×8 array at various operating frequency points. (a) in the elevation plane. (b) in the azimuth plane.

The power divider should have low insertion loss, and maximum energy should be available at each output port (i.e., input of sub-array antenna) with equal magnitude and phase. The consistency in the magnitude and phase of the transmission coefficients (S_{21} , S_{31} , S_{41} , and so on) of a power divider is crucial for the reliable transmission of data packets as well as to guarantee the accurate delivery of signals to the nodes of Industrial IoT network [28]. Note that in case of an 8-way equal power divider, $1/8$ of the total power (equivalent to -9.03 dB) should ideally be available to each output port (port 2 to port 9). As shown in Fig. 11(b), the insertion loss of the power divider is within -9.6 to -10.1 dB, whereas the reflection coefficient ($|S_{11}|$) is maintained to be less than -10 dB within the desired band.

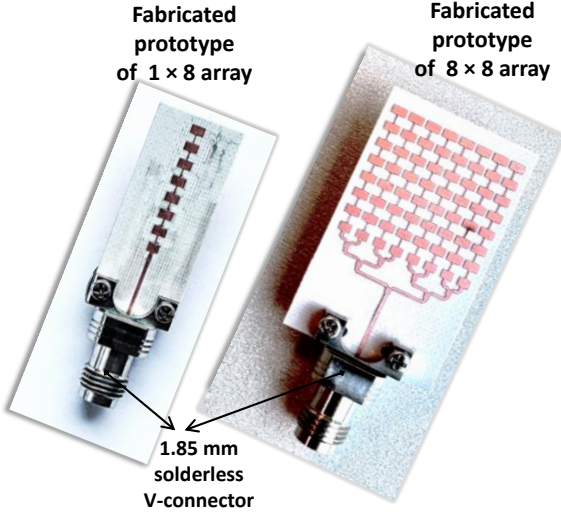


Fig. 15. Fabricated prototypes of the proposed antenna arrays.

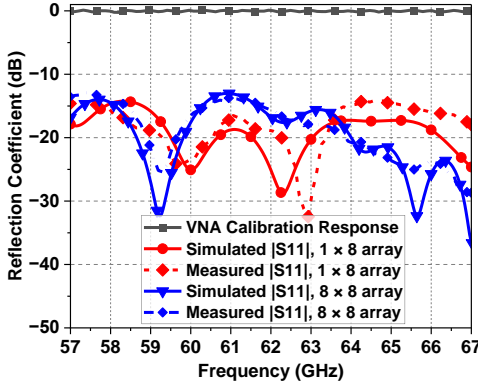


Fig. 16. Measured reflection coefficient of the proposed 1×8 and 8×8 arrays.

The 3-D schematic and perspective of the proposed 64-element (8×8) array is shown in Fig. 12(a). Fig. 12(b) reveals u-v projections of the radiation patterns which elucidates frequency beam-scanning. The simulated reflection coefficient and realized gain are shown in Fig. 13. The array is linearly polarized and provides the peak simulated gain of 20.36 dBi at 64 GHz, whereas the simulated gain is above 19.36 dBi in 57–71 GHz band, thus high gain flatness is achieved with 1dB gain BW of 14 GHz.

2-D radiation patterns in the elevation and azimuth planes are shown in Fig. 14. High-gain directional radiation patterns with narrow beamwidth in both azimuth and elevation planes are achieved. Within 57–71 GHz, the simulated HPBW varies between 10.87° to 13.14° in the azimuth plane and 7.86° to 10.98° in the elevation plane. The direction of the main lobe is towards $\phi=0^\circ$ in the azimuth plane. The sidelobe levels are below -10 dB, and x-pol levels are low as depicted in Fig. 14. The radiation efficiency of 8×8 array is above 83.31% in 57–71 GHz band.

IV. PROTOTYPE FABRICATION AND MEASUREMENT RESULTS

The fabricated prototypes of the proposed 1×8 (sub-array) and 8×8 (64-element) arrays are shown in Fig. 15. The size of the 8×8 array including the power divider is 20 mm ($4\lambda_0$)

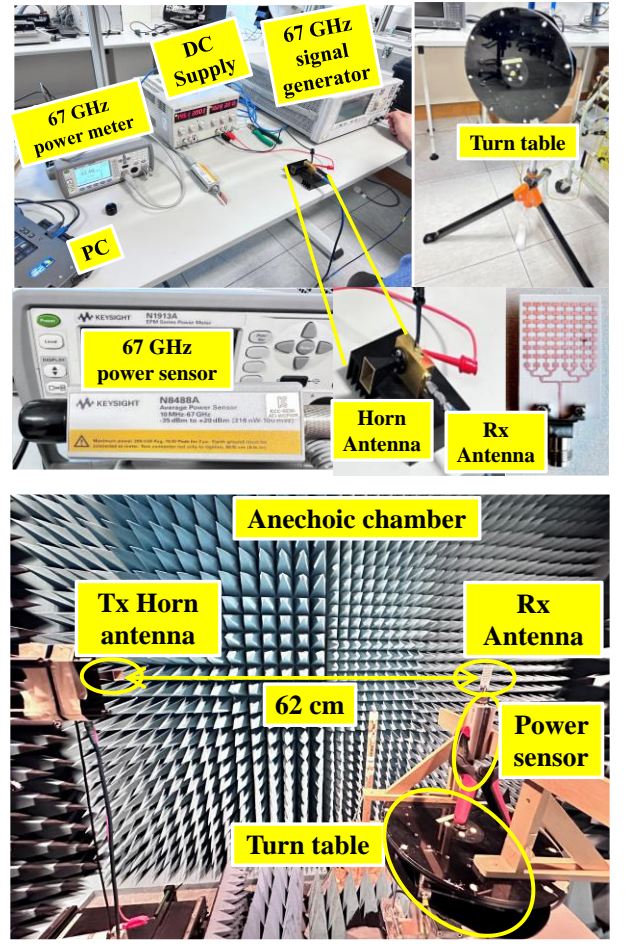


Fig. 17. (Top) Measurement equipment utilized for experimental verification. (bottom) Measurement setup to test the radiation pattern and gain in the anechoic chamber.

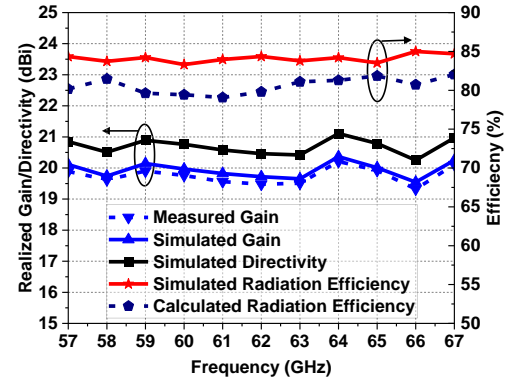


Fig. 18. Measured gain, and radiation efficiency of the proposed 8×8 array.

$\times 28$ mm ($5.6\lambda_0$) $\times 0.25$ mm ($0.05\lambda_0$), where λ_0 is free space

wavelength at 60 GHz. To excite the antenna array, an edge-launched solderless 1.85 mm standard V-connector was used for ease of measurement. As soldering is not required in this type of connector, the loss due to the deposition of copper during the soldering process is avoided (as it might adversely affect the performance at 60 GHz). Here, it is instructive to

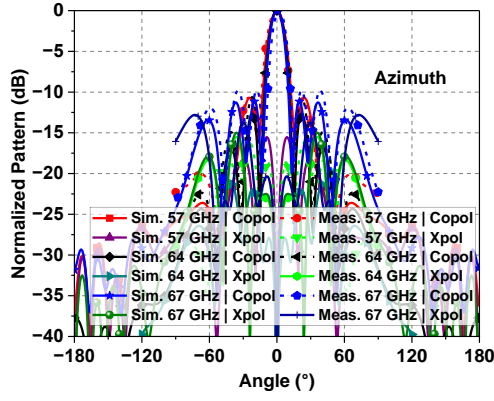


Fig. 19. Measured radiation patterns of 8×8 array at 57, 64, and 67 GHz in the azimuth plane.

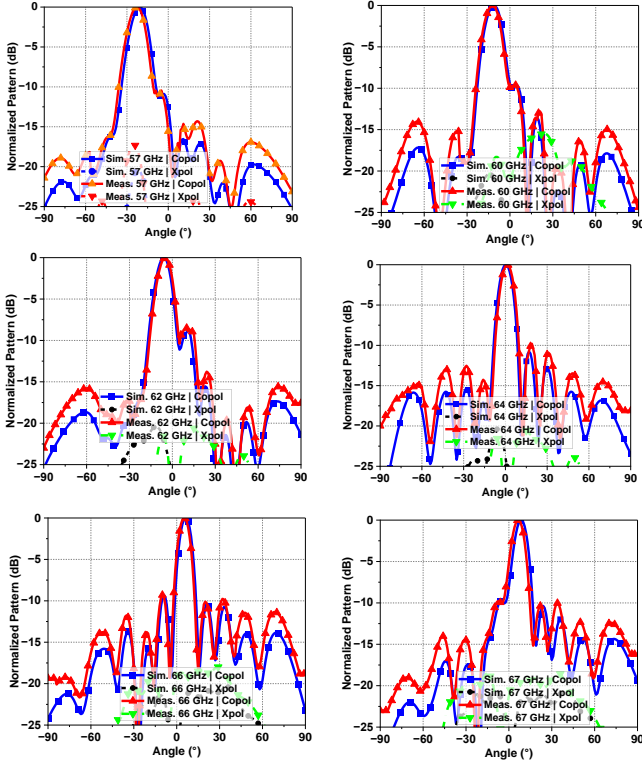


Fig. 20. Measured radiation patterns of 8×8 array at 57, 60, 62, 64, 66, and 67 GHz in the elevation plane.

mention that we utilized 1.85 mm standard RF equipment in our measurement setup, which has a maximum supported frequency of 67 GHz. Consequently, the measured results are presented here within 57–67 GHz range.

The measured -10 dB impedance BW of the proposed 1×8 and 8×8 arrays match reasonably well with simulations, as shown in Fig. 16. Some discrepancies are mainly due to fabrication tolerance and surface roughness.

The measured -10 dB impedance BW of the proposed 1×8 and 8×8 arrays match reasonably well with simulations, as shown in Fig. 16. Some discrepancies are mainly due to fabrication tolerance and surface roughness. The measurement setup for the radiation pattern and gain measurements consists of a 67 GHz signal generator, V-band standard gain horn antennas, the proposed array as Rx antenna, 67 GHz power

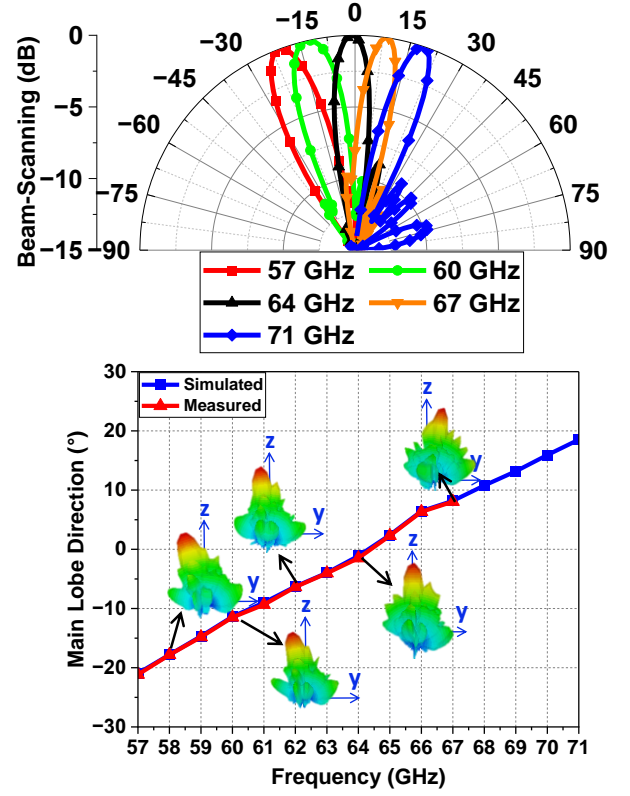


Fig. 21. Measured frequency beam-scanning performance of 8×8 array in the elevation plane demonstrated in polar form (top) and 3-D form with main lobe direction (bottom).

meter and power sensor, a turn table for antenna rotation, and a PC for automation and data acquisition.

The measurement setup was placed in an anechoic chamber to minimize any possible ambient reflections, as shown in Fig. 17. The distance between the Tx and Rx antennas was set as 62 cm to satisfy the far-field condition. Since we aim to design a wideband high-gain compact array, therefore onwards we present the measured gain and radiation patterns of the 8×8 array due to brevity (the measured gain and radiation patterns of 1×8 array were observed in good agreement with the simulations, validated by measured S11 in Fig. 16).

The gain was measured using the gain comparison method using a standard gain V-band horn antenna. Two sets of measurements were performed with a 1 GHz step in 57–67 band. In one set, the received power with a standard gain horn antenna (P_{horn}) was measured, whereas in the other set, the received power with 8×8 array (P_{array}) was measured. At each test frequency, the gain (in dB scale) was calculated by $G_{array(dB)} = G_{horn(dB)} - (P_{horn(dB)} - P_T) + (P_{array(dB)} - P_T)$, where G_{array} is the measured gain of the array at a fixed frequency, G_{horn} is the known/given gain of the standard gain horn antenna at that frequency, while P_T is the transmit power. Fig. 18 shows the measured gain, directivity, and radiation efficiency of the proposed 8×8 array. The peak measured gain of 20.12 dBi is achieved at 64 GHz. The measured gain is above 19.23 dBi throughout the band of interest, thereby providing a measured 1 dB gain-BW of 14 GHz. Such flat gain over a wide BW is the hallmark of the proposed antenna design. The calculated radiation efficiency was found

TABLE I.

PERFORMANCE COMPARISON OF THE PROPOSED WORK WITH CLOSELY RELATED 60 GHz ANTENNAS

Ref.	Array Type and Geometry	-10 dB BW (FBW %)	Peak Gain (dBi)/ Gain Variation in 57-71 GHz	Beam-scanning (Scanning Range)	Size (mm) (W × L × H) (*λ=5mm at 60 GHz)
[12]	SIW planar leaky wave slot array 1 × 8	55–65 (16.66 %)	14.5 (> 3 dB)	Yes -72° to +48°	23 × 38 × 0.38 (4.6λ × 7.6λ × 0.07λ)
[18]	Planar SIW slot array 12 × 12	59.3–61.8 (4.12 %)	22 (> 3 dB)	No	NA × NA × 0.51 (*λ × *λ × 0.102λ)
[20]	SIW multilayer PCB 1 × 4	50.79–70.85 (33 %)	11.9 (> 3 dB)	No	22 × 25 × 1.05 (4.4λ × 5λ × 0.21λ)
[21]	Series-fed microstrip patch array 1 × 4	57–66 (14.63 %)	14.5 (< 1 dB)	No	14.7 × 6 × 0.25 (2.94λ × 1.2λ × 0.04λ)
[22]	Microstrip dipoles 1 × 4	57–64 (10.69 %)	16.5 (> 3 dB)	No	18.5 × 30 × 0.25 (3.7λ × 6λ × 0.05λ)
[24]	Parallel-series fed microstrip patch array 8 × 4	58–60.5 (4.22 %)	18 (Not given)	No	35 × 35 × 0.1 (7λ × 7λ × 0.02λ)
[25]	Series-fed microstrip patch array 2 × 10	58.5–62 (4.2 %)	16.4 (> 3 dB)	Partial, at two angles only. -20° and +20°	× 30 × 0.51 (3.7λ × 6λ × 0.102λ)
This Work	Series-fed linear array 1 × 8	54–82.3 (41.52%, sim.) 54–67 (meas. presented)	13.48 (< 1 dB)	Yes -23° to +17°	13 × 23 × 0.25 (2.6λ × 4.6λ × 0.05λ)
	Parallel-series planar array 8 × 8	49.28–73 (38.79%, sim.) 49.28–67 (meas. presented)	20.36 (< 1 dB)	Yes -21° to +19°	20 × 28 × 0.25 (4λ × 5.6λ × 0.05λ)

using the measured gain and simulated directivity as

$$Cal. Rad. Eff. = \frac{Measured Gain}{Simulated Directivity}.$$

The radiation patterns were measured in both azimuth and elevation planes in 1° resolution from -90° to +90°. The measured radiation pattern in the azimuth plane (x-z/Phi 0°) at 57, 64, and 67 GHz is shown in Fig. 19. The measured HPBW varies well with the simulated results. The main beam direction in azimuth plane is towards 0° across 57–71 GHz band. The SLLs are below -10 dB and x-pol levels are below -30 dB in the direction of main lobe, as shown in Fig. 19. The measured radiation patterns in the elevation plane at various frequency points in 57-67 GHz band are shown in Fig. 20. The measured HPBW ranges between 8.1° to 10.8° from 57–67 GHz in the elevation plane. SLL is less than -10 dB and x-pol levels are below -20 dB. Fig. 21 demonstrates the measured frequency beam-scanning performance of the proposed 8 × 8 array in the elevation plane.

Table I compares the performance of the proposed array design with other closely related antenna arrays at 60 GHz band in the literature. It can be noticed that the proposed array outperforms various other designs in terms of high-performance indicators such as wide impedance BW, and high flat gain while maintaining a compact size.

V. CONCLUSION

A compact, wideband, and planar series-fed 1 × 8 linear microstrip sub-array is proposed to support the entire 57–71 GHz ISM band with high gain. The linear array has peak gain of 13.48 dBi at 64 GHz and provides less than 1 dB gain variation in 57–71 GHz. The proposed array manifests frequency beam-scanning over the scanning range of 40°. Based on the proposed linear sub-array, eight such arrays were employed to design a compact planar 64-element (8 × 8) array using a hybrid parallel-series topology. The planar array provides a peak measured realized gain of 20.12 dBi at 64 GHz, with less than 1 dB gain variation over 14 GHz band from 57–71 GHz. The size of 64-element array is 2 cm × 2.8 cm. The array prototypes are fabricated and measured. The proposed wideband antenna array is a suitable candidate for numerous emerging mmWave industrial wireless applications in context of Industry 4.0 and Industry 5.0, as well as 60 GHz FMCW radars. The array is compatible to work with various 60 GHz physical layer protocols such as IEEE 802.11ay, IEEE 802.11ad, IEEE 802.15.3c, WirelessHD, and ECMA-387 as well as other customized industrial protocols such as WirelessHP.

The proposed wideband high-gain array is potentially applicable in mmWave industrial localization, sensing, and product tracking systems. FMCW radar systems utilize a frequency-swept signal to attain precise range measurements while avoiding short, high-energy pulses. By comparing the instantaneous radio frequency of both the transmitted and received signals, a periodic FMCW signal can ascertain the time of flight and, consequently, the range of the radar system's target.

Furthermore, the proposed 1 × 8 array can be employed to develop multiple-input-multiple-output (MIMO) array for digital beamforming. Instead of a single parallel feed to each designed sub-array (analog beamforming as in this work), each sub-array can be separately fed to create digital beamforming. Besides, such configuration can be integrated with a V-band phase shifting mechanism to devise a mmWave digital MIMO beamforming system. MIMO arrays possess promising potential to connect various IIoT devices with high reliability, spatial diversity, and high energy efficiency.

REFERENCES

- [1] Z. Pang, M. Luvisotto, and D. Dzung, "Wireless high-performance communications: The challenges and opportunities of a new target," *IEEE Ind. Electron. Mag.*, vol. 11, no. 3, pp. 20–25, 2017.
- [2] S. Saponara, F. Giannetti, B. Neri, and G. Anastasi, "Exploiting mm-wave communications to boost the performance of industrial wireless networks," *IEEE Trans. Ind. Informatics*, vol. 13, no. 3, pp. 1460–1470, 2017.
- [3] R. Jacobi and A. Aginskiy, "Choosing 60-GHz mmWave sensors over 24-GHz to enable smarter industrial applications," *Nov 2018, Texas Instruments*, 2018.
- [4] L. Da Xu, W. He, and S. Li, "Internet of things in industries: A survey," *IEEE Trans. Ind. Informatics*, vol. 10, no. 4, pp. 2233–2243, 2014.
- [5] T. Kalsoom *et al.*, "Impact of IOT on Manufacturing Industry 4.0: A new triangular systematic review," *Sustainability*, vol. 13, no. 22, p. 12506, 2021.

- [6] A. Mahmood *et al.*, "Industrial IoT in 5G-and-beyond networks: Vision, architecture, and design trends," *IEEE Trans. Ind. Informatics*, vol. 18, no. 6, pp. 4122–4137, 2021.
- [7] E. Sisinni, A. Saifullah, S. Han, U. Jennehag, and M. Gidlund, "Industrial internet of things: Challenges, opportunities, and directions," *IEEE Trans. Ind. Informatics*, vol. 14, no. 11, pp. 4724–4734, 2018.
- [8] X. Xu, Y. Lu, B. Vogel-Heuser, and L. Wang, "Industry 4.0 and Industry 5.0—Inception, conception and perception," *J. Manuf. Syst.*, vol. 61, pp. 530–535, 2021.
- [9] M. Cheffena, "Industrial wireless communications over the millimeter wave spectrum: opportunities and challenges," *IEEE Commun. Mag.*, vol. 54, no. 9, pp. 66–72, 2016.
- [10] C. Pielli, T. Ropitault, and M. Zorzi, "The potential of mmwaves in smart industry: Manufacturing at 60 ghz," in *International Conference on Ad-Hoc Networks and Wireless*, Springer International Publishing, 2018, pp. 64–76. doi: 10.1007/978-3-030-00247-3_6.
- [11] A. Jabbar *et al.*, "Millimeter-Wave Smart Antenna Solutions for URLLC in Industry 4.0 and Beyond," *Sensors*, vol. 22, no. 7, p. 2688, 2022, doi: 10.3390/s22072688.
- [12] A. Sarkar and S. Lim, "60 GHz compact larger beam scanning range PCB leaky-wave antenna using HMSIW for millimeter-wave applications," *IEEE Trans. Antennas Propag.*, vol. 68, no. 8, pp. 5816–5826, 2020.
- [13] J. Li, C. Matos, and N. Ghalichechian, "A Low-Cost Vertically Integrated Antenna Array at 60 GHz With 85% Efficiency," *IEEE Antennas Wirel. Propag. Lett.*, vol. 20, no. 4, pp. 513–517, 2021.
- [14] S. D. Joseph and E. A. Ball, "Series-Fed Millimeter-Wave Antenna Array Based on Microstrip Line Structure," *IEEE Open J. Antennas Propag.*, vol. 4, pp. 254–261, 2023.
- [15] A. Attaran, R. Rashidzadeh, and R. Muscedere, "Rotman lens combined with wide bandwidth antenna array for 60 GHz RFID applications," *Int. J. Microw. Wirel. Technol.*, vol. 9, no. 1, pp. 219–225, 2017.
- [16] B. Biglarbegian, M. Fakharzadeh, D. Busuioac, M.-R. R. Nezhad-Ahmadi, and S. Safavi-Naeini, "Optimized microstrip antenna arrays for emerging millimeter-wave wireless applications," *IEEE Trans. Antennas Propag.*, vol. 59, no. 5, pp. 1742–1747, 2011, doi: 10.1109/TAP.2011.2123058.
- [17] H. Chu, J.-X. Chen, and Y.-X. Guo, "An efficient gain enhancement approach for 60-GHz antenna using fully integrated vertical metallic walls in LTCC," *IEEE Trans. Antennas Propag.*, vol. 64, no. 10, pp. 4513–4518, 2016.
- [18] X.-P. Chen, K. Wu, L. Han, and F. He, "Low-cost high gain planar antenna array for 60-GHz band applications," *IEEE Trans. Antennas Propag.*, vol. 58, no. 6, pp. 2126–2129, 2010.
- [19] P. Cabrol and P. Pietraski, "60 GHz patch antenna array on low cost Liquid-Crystal Polymer (LCP) substrate," in *IEEE Long Island Systems, Applications and Technology (LISAT) Conference 2014*, 2014, pp. 1–6.
- [20] J. Zhang, X. Zhang, and A. A. Kishk, "Broadband 60 GHz antennas fed by substrate integrated gap waveguides," *IEEE Trans. Antennas Propag.*, vol. 66, no. 7, pp. 3261–3270, 2018.
- [21] T. H. Jang, H. Y. Kim, I. S. Song, C. J. Lee, J. H. Lee, and C. S. Park, "A wideband aperture efficient 60-GHz series-fed E-shaped patch antenna array with copolarized parasitic patches," *IEEE Trans. Antennas Propag.*, vol. 64, no. 12, pp. 5518–5521, 2016.
- [22] Y. Al-Alem and A. A. Kishk, "Efficient millimeter-wave antenna based on the exploitation of microstrip line discontinuity radiation," *IEEE Trans. Antennas Propag.*, vol. 66, no. 6, pp. 2844–2852, 2018.
- [23] W. Yang, K. Ma, K. S. Yeo, and W. M. Lim, "A compact high-performance patch antenna array for 60-GHz applications," *IEEE Antennas Wirel. Propag. Lett.*, vol. 15, pp. 313–316, 2015, doi: 10.1109/LAWP.2015.2443054.
- [24] J. Säily, A. Lamminen, and J. Francey, "Low cost high gain antenna arrays for 60 GHz millimetre wave identification (MMID)," in *Sixth ESA Workshop on Millimetre-Wave Technology and Applications-Fourth Global Symposium Millimetre Waves, Espoo, Finland*, 2011.
- [25] Y. Liu *et al.*, "Design and fabrication of two-port three-beam switched beam antenna array for 60 GHz communication," *IET Microwaves, Antennas & Propag.*, vol. 13, no. 9, pp. 1438–1442, 2019.
- [26] C. A. Balanis, *Antenna theory: analysis and design*. John Wiley & sons, 2015.
- [27] A. Jabbar, Z. Pang, G. A. Safdar, Q. Abbasi, M. A. Imran, and M. Ur-Rehman, "A Compact Wideband Millimeter-Wave Beam-Scanning Antenna Array for Industry 4.0 and Beyond Applications," *2023 IEEE Int. Work. Antenna Technol.*, pp. 1–4, 2023.
- [28] S. Pan, M. Lin, M. Xu, S. Zhu, L.-A. Bian, and G. Li, "A low-profile programmable beam scanning holographic array antenna without phase shifters," *IEEE Internet Things J.*, 2021.